Supporting Information

A Magnetically Controlled Guidewire Robot System with Steering and Propulsion Capabilities for Vascular Interventional Surgery

Shixiong Fu, Binghan Chen, Dong Li, Jianguo Han, Sheng Xu, Shu Wang, Chenyang Huang, Ming Qiu, Si Cheng, Xinyu Wu, Li Zhang, Shiwei Du, and Tiantian Xu**

This file includes:

Supplementary Videos

Supplementary Figures

Supplementary Tables

Supplementary Videos

Video S1. Trajectory Following of the Magnetically Controlled Guidewire Robot System (MCGRS) in Three Different Vascular Phantoms

Video S2. In Vitro Navigation validation of the Magnetically Controlled Guidewire Robot System (MCGRS) in 3D Vascular Phantom

Video S3. In Vitro Verification of the Magnetically Controlled Guidewire Robot System (MCGRS) under X-ray Fluorescence Imaging

Supplementary Figures

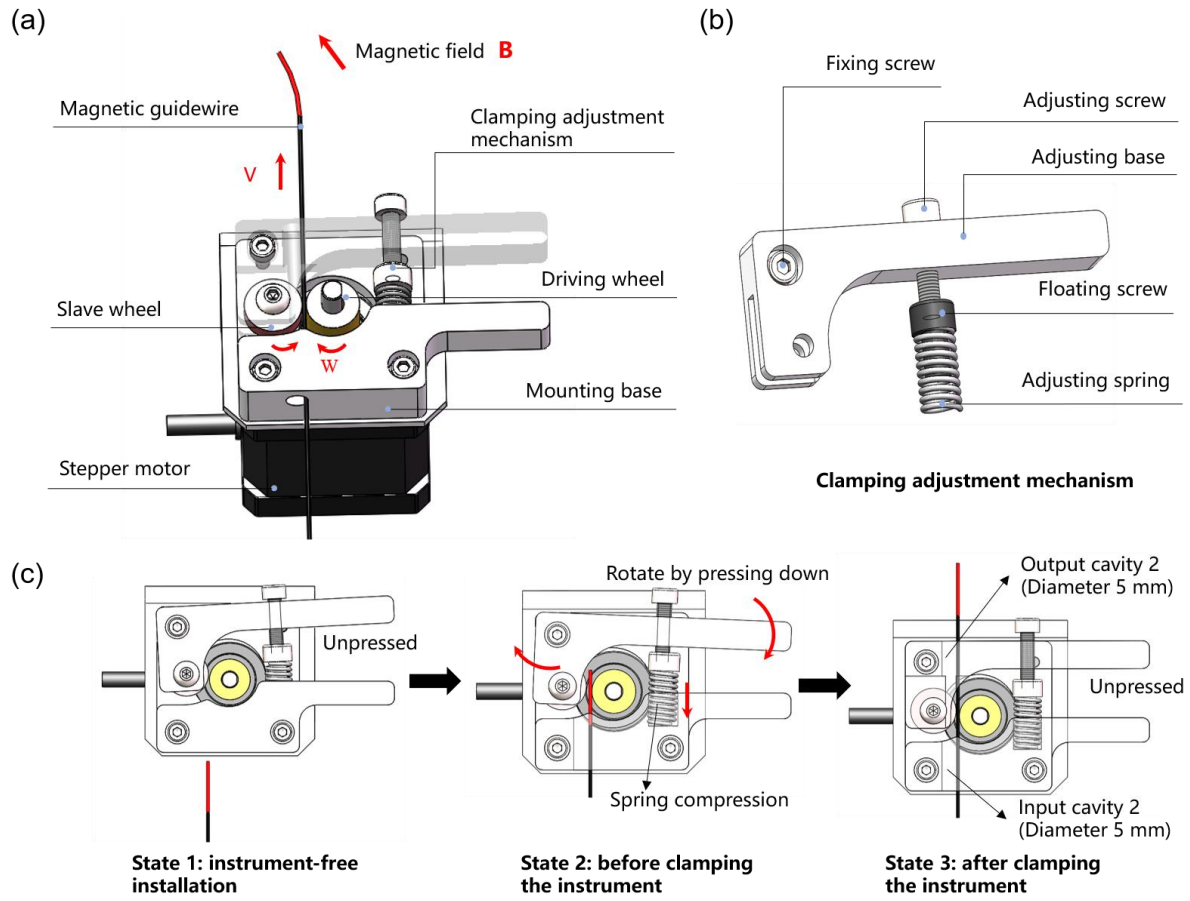

Figure S1. The linear propulsion module and the instrument installation process of the guidewire/catheter advancer (GCA). (a) the detailed structure illustration of the guidewire advancer in the GCA. (b) The detailed compositional structure of the clamping adjustment mechanism in (a). (c) The instrument installation process and the state comparison of the before/after clamping the instrument. The red arrows in the figure indicate the direction of component motion and the direction of the external magnetic field.

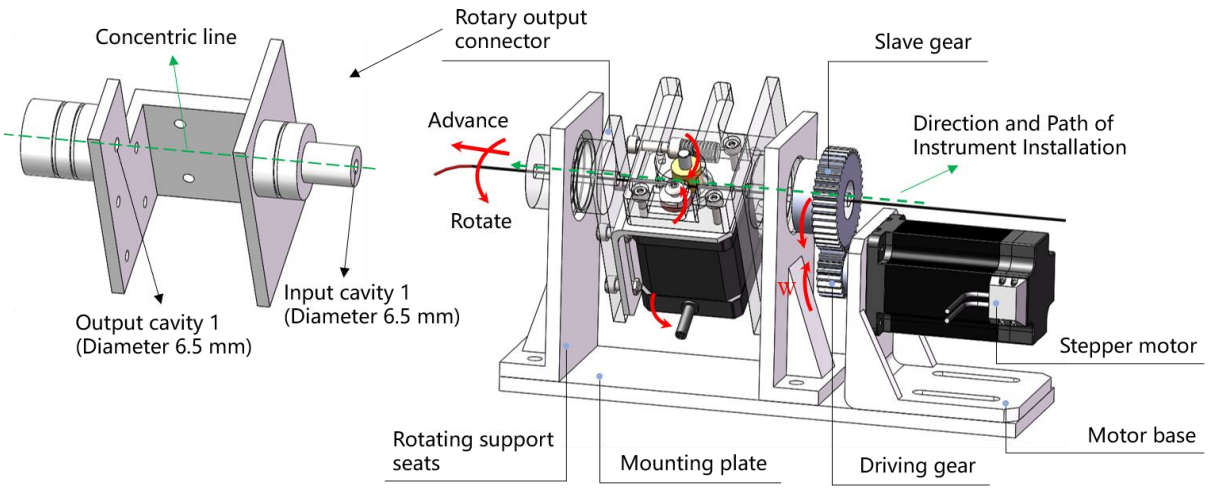

Figure S2. Diagram of the structural components of the rotary motion module and the operating schematic of simultaneous linear and rotary motion of the guidewire/catheter advancer (GCA). The red arrow in the right figure indicates the direction of motion, and the green dotted line indicates the direction and path of the instrument installation. The left figure indicates the structure of the rotary output connector, and the green dashed line indicates the concentric line.

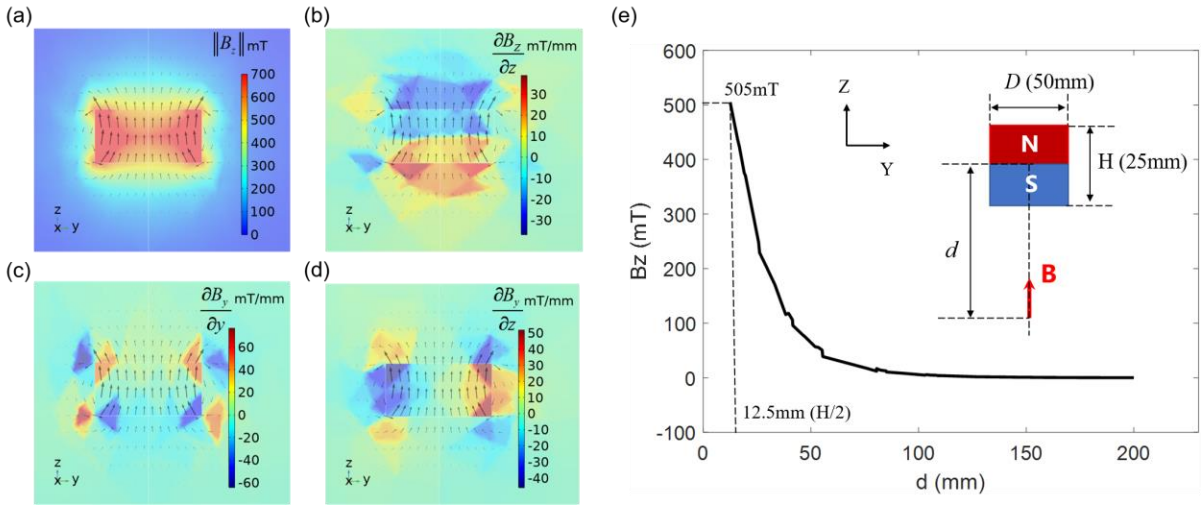

Figure S3. Magnetic field characterization of external permanent magnet. (a)-(d) The magnitude distribution of the magnetic field strength and non-zero magnetic field gradient along the Z-axis of the magnet center. (e) The variation relationship between the magnetic field strength Bz in the central axis and the normal working distance d from the magnetic field center-of-mass point to the magnetic tip action point.

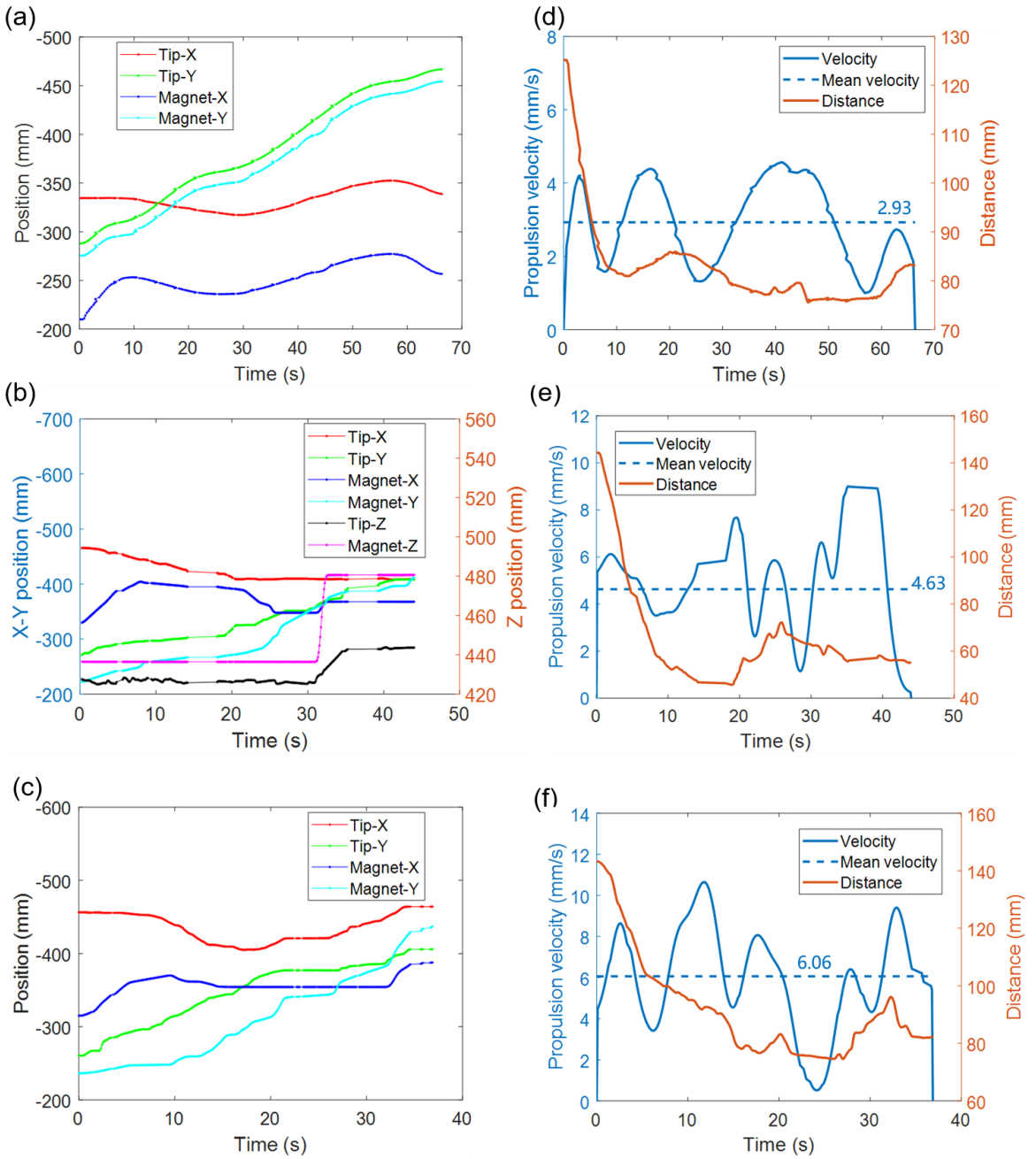

Figure S4. Curves of magnet and tip positions, relative distances, and tip velocities over time in the three trajectory following experiments. (a)-(c) Position curves of the magnetic tip and external magnets over time for the three trajectory following experiments, respectively. (d)-(f) Actual variation curves of the distance from the magnet to the magnetic tip and the propulsion velocity of magnetic tip with time for the three trajectory following experiments, respectively.

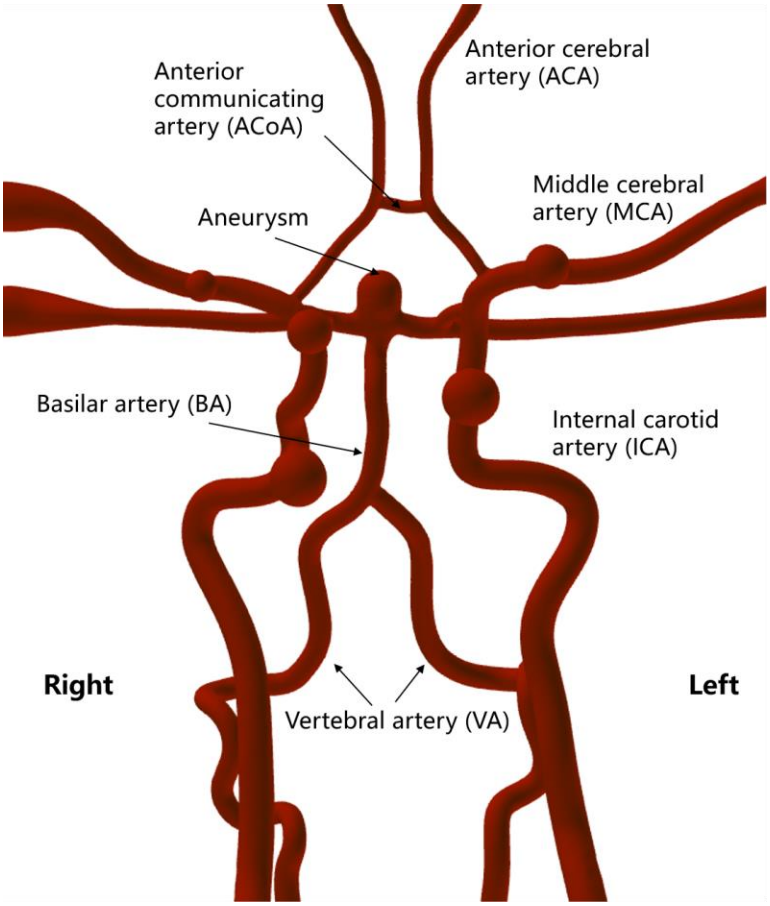

Figure S5. The anatomy and nomenclature of the intracranial artery of the adopted phantom in our study. The overall intracranial artery consists of two parts, the left and right, each consisting mainly of Vertebral artery (VA), Internal carotid artery (ICA), Basilar artery (BA), Middle cerebral artery (MCA), Anterior communicating artery (ACoA), Anterior cerebral artery (ACA), and several Aneurysms.

Supplementary Tables

Table S1. Parameters of the permanent magnet in the MAS

Parameters	Value
Material	NdFeB（N52）
Density [kg/m3]	7500
Diameter [mm]	50
Length[mm]	25
Remanence [mT]	1440
Maximum magnetic flux density [mT]	505

Table S2. Parameters of the magnetic tip

Items	Parameters	Value
Tip magnets	Material	NdFeB（N52）
	Density [kg/m3]	7500
	Diameter [mm]	0.5
	Length[mm]	2.5
	Amount	2
	Remanence [mT]	1440
PDMS elastic segment	Material	Polydimethylsiloxane
	Density [kg/m3]	0.97
	Diameter [mm]	0.5
	Length[mm]	≥5
Silicone tube	Material	Silicone
	Density [kg/m3]	1200
	Inner diameter [mm]	0.5
	Outer diameter [mm]	1
	Length[mm]	≥12